

Probabilistically Shaped PAM-8 Transmission With Simplified Volterra Equalizer

Mingyi Gao , Mengli Liu, Junchi Ke, and Bowen Chen 

Abstract—Intensity-modulation direct-detection (IM/DD) probabilistically shaped (PS) 8-level pulse-amplitude modulation (PAM) signal is promising for high-speed intra-data-center networks. However, the challenges of a PS-PAM-8 transmission system are complicated distribution matcher (DM) and nonlinear equalizer. In this work, we propose a simple PS-PAM-8 transmission system, where the probabilistic amplitude shaping (PAS) encoder consists of an energy-level-assigned (ELA)-based DM and a low-density parity-check (LDPC) encoder. In the ELA-based DM, a simple lookup table is designed to realize an approximate bilateral Maxwell-Boltzmann distribution by assigning energy levels to various symbols. Consequently, the DM encoded bits are used as the amplitude bits, and DM label bits and LDPC check bits are designated as sign bits to implement PAS encoding. In addition, a simplified Volterra equalizer (SVE) is introduced to eliminate the inter-symbol interference and improve the receiver sensitivity of PS-PAM-8 signal, where the SVE only includes the 2-order kernel to reduce its complexity. We experimentally demonstrated the proposed PS-PAM-8 scheme and verified its outperformance over uniform PAM-8 signal in the back-to-back and 2-km standard single mode fiber (SSMF) transmission. Compared to the conventional linear equalizer, the SVE contributes approximate 1-dB improvement of the receiver sensitivity in the PS-PAM-8 2-km SSMF transmission, for the error-free performance of post forward error correction bit error ratio.

Index Terms—Probabilistic shaping, pulse-amplitude modulation, Volterra equalizer.

I. INTRODUCTION

TO HANDLE the large-capacity connections within the data centers, intra-data-center (IDC) networks require high-speed optical interconnects with the low complexity. Intensity-modulation direct-detection (IM/DD) technology has advantages over coherent technology due to its simpler and low-cost components [1], [2], [3]. Among various advanced modulation formats, pulse-amplitude modulation (PAM) signals have a simpler implementation and higher spectral efficiency, and high-speed PAM-4 signals have been investigated widely [4], [5], [6], [7], [8].

Manuscript received 15 November 2022; accepted 18 November 2022. Date of publication 28 November 2022; date of current version 8 December 2022. This work was supported by the National Natural Science Foundation of China Project under Grant 62075147. (Corresponding author: Mingyi Gao.)

The authors are with the Jiangsu Engineering Research Center of Novel Optical Fiber Technology and Communication Network, Suzhou Key Laboratory of Advanced Optical Communication Network Technology, the School of Electronic and Information Engineering, Soochow University, Suzhou, Jiangsu 215006, China (e-mail: mygao@suda.edu.cn; 20195228009@stu.suda.edu.cn; 20205228058@stu.suda.edu.cn; bwchen@suda.edu.cn).

Digital Object Identifier 10.1109/JPHOT.2022.3224205

In comparison with PAM-4 signals, PAM-8 signals can carry more information at the expense of more complicated digital signal processing (DSP), and probabilistic shaping (PS) and nonlinear equalizers were exploited to enhance the robustness of PAM-8 signals [9], [10], [11], [12], [13], [14]. Furthermore, when the modulation amplitude is increased to PAM-16, the nonlinear equalization becomes more challenging for compensating the critical nonlinear impairments caused by the electro-optical components in the nonlinear operating region [15], [16], [17]. However, it is significant for future large-capacity IDC to investigate the PAM-8 and PAM-16 schemes. After the probabilistically shaped PAM-8 (PS-PAM-8) system has been first experimentally demonstrated, several state-of-the-art works have been reported to show the outperformance of PS-PAM-8 signals [9], [10], [11], [12]. Furthermore, a probabilistic amplitude shaping (PAS) scheme was proposed by integrating PS and forward error correction (FEC) to combine the distribution matcher (DM) with the systematic encoder of binary low-density parity-check (LDPC) codes [18], [19]. The PAS architecture can achieve the PS and FEC encoding efficiently and in such a joint coding scheme, the complexity of the system mainly relies on that of the DM. Many DM algorithms for high-order quadrature amplitude modulation signals have been proposed, such as product distribution matching, hierarchical distribution matching, constant composition distribution matching (CCDM), m-out-of-n DM and prefix-free code distribution matching etc. [18], [19], [20], [21], [22], [23], [24]. Here, CCDM is widely used due to its characteristic of approaching the desired probabilistic distribution, however, long block lengths are required and the complexity is an issue. By comparison, the cut-and-paste (CAP)-based DM with lower complexity, is promising for PS-PAM signals [25]. In the CAP-based DM, a transmitted sequence is divided into many n-symbol segments and for each n-symbol segment, after the bit-to-symbol mapping, the amplitude bits are extracted and inverted. However, the CAP-based DM needs many multipliers and comparators because twice mappings are implemented to select sequences with lower energy. Moreover, for a fixed n-symbol encoding, the chosen sequences with lower energy always have a lower information rate and a determined distribution. To yield a flexible configuration of probability distributions, we proposed an energy-level-assigned (ELA)-based DM for PS-PAM-4 signals by pre-calculating and assigning energy levels [26]. The ELA-based DM is a simple method to achieve a desired probability distribution and suitable for the PS-PAM-8 transmission system with low complexity.

Furthermore, a simple equalizer is indispensable in the PAM-8 transmission to mitigate the inter symbol interference (ISI) [27]. Generally, feed-forward equalizer (FFE) is effective to eliminate linear ISI, while Volterra equalizer (VE) is used to mitigate both linear and nonlinear ISI [28], [29], [30], [31]. Although, both of FFE and VE can alleviate the power fading caused by bandwidth limitations and chromatic dispersion, the noise components are simultaneously increased. In addition, decision feedback equalizer (DFE) can compensate the spectral notches caused by fiber chromatic dispersion, but error propagation is caused by the hard decision module. Therefore, it is challenging to implement the cascaded DFE and FEC decoder [31], [32]. Meanwhile, maximum likelihood sequence estimation (MLSE) suppresses the noise components enhanced by FFE and VE through a post-filter, where Viterbi decoding is utilized to yield judgment symbols [33], [34]. However, when FEC decoder is appended, error propagation is still an open issue in the MLSE due to the required hard decision module of Viterbi algorithm. MLSE algorithm with the soft decision was proposed for PAM-4 signal transmission [35]. Unfortunately, the computational complexity of MLSE is overwhelming and increases exponentially with the channel memory length. Moreover, in bandwidth-constrained PAM systems, Tomlinson-Harashima precoding (THP) was used to improve the performance [36], [37], [38]. However, THP can't be directly appended to the PS-PAM system because the output signal of the nonlinear modulo operation in the feedforward path of the pre-encoder is random to a certain extent, thus corrupting the Maxwell-Boltzmann (MB) distribution generated by the PS encoder [32]. To escape the dilemma of equalizers' performance and computational complexity in the PS-PAM transmission, a simplified Volterra equalizer (SVE) is a good candidate for joint coding of PS and FEC with moderate complexity to mitigate both linear ISI and nonlinear ISI.

In this work, we propose and experimentally demonstrated a PS-PAM-8 transmission system based on a joint coding of ELA-based DM and LDPC. The PS-PAM-8 signal outperforms the uniform PAM-8 (UN-PAM-8) signal at the same net bit rate, where the signal isn't heavily bandwidth restricted. In addition, we utilized a SVE in the PS-PAM-8 experiment, where only the kernels of 2-order VE are remained. We measured the post-FEC bit error ratio (BER) and post-ELA BER curves and achieved 2-dB and 1-dB improvements of receiver sensitivity by comparison with the conventional FFE in the back-to-back (BTB) and 2-km transmission, respectively.

The structure of the paper is organized as follows. In Section II, we first introduced the principle of PAS with ELA-based DM and LDPC for PS-PAM-8 signal. Then we analyzed the channel impairment of IM/DD system and illustrated the implementation of the SVE. In Section III, we presented the experimental setup and discussed the experimental results, where the number of taps for the equalizer was optimized and the complexity was analyzed. Finally, we summarized the paper in Section IV.

II. PRINCIPLE

In the IM/DD PAM-8 system, the symbols with higher amplitude levels always suffer from more serious degradation.

Thus, for the PS-PAM-8 signal, the degradation is mitigated by decreasing the occurrence probability of symbols with higher amplitude levels and increasing that of symbols with lower amplitude levels. To implement the PAS scheme, the ELA-based DM is used to obtain the shaped amplitude bit sequence and the LDPC with systematic encoding is selected as the FEC. Additional label bits are required to indicate the behavior of the bit inversion for the ELA-based DM. The error propagation will be induced by the errors of the label bits and thus it is significant to keep the label bits undistorted. Meanwhile, the sign bits are resilient to noise during transmission. The label bits generated in the DM and the check bits generated in the LDPC encoding, can be exploited as the sign bits to ensure the accuracy of the label bits and the check bits [18], [26]. In the following experiments, the post-FEC BER and the post-ELA BER are measured to verify the robustness to the error propagation of the proposed scheme.

Fig. 1 shows the architecture of the PS-PAM-8 transmission system with the joint coding of ELA-based DM and LDPC, which includes the ELA encoder, LDPC encoder, PAM-8 symbol mapping, channel transmission, log likelihood ratio (LLR) calculation module, LDPC decoder and ELA decoder. Here, the uniform random bit sequence \mathbf{U}_1 first enters the ELA encoder to obtain the reshaped bit sequence $\mathbf{b}(\mathbf{A})$ and the uniform label bit sequence \mathbf{L} . Besides, \mathbf{A} represents the amplitude level sequence after PS, which only contains amplitude bit information. For each PAM- M symbol, each amplitude level in sequence \mathbf{A} contains $m-1$ bits, where $m = \log_2(M)$. Afterwards, the uniform random bit sequence \mathbf{U}_2 , together with $\mathbf{b}(\mathbf{A})$ and \mathbf{L} , is launched to the LDPC encoder.

Then the parity bit sequence \mathbf{P} , \mathbf{L} and \mathbf{U}_2 generated by the LDPC encoder together serve as the sign bits \mathbf{S} in the PAM-8 symbol, and the non-uniformly distributed bit sequence $\mathbf{b}(\mathbf{A})$ is used as the amplitude bits for PAM-8 symbol. After PAM-8 symbol mapping, the symbol sequence \mathbf{X} is generated.

Next, the received sequence \mathbf{Y} is obtained after channel transmission. Then, LLR estimation is implemented to obtain soft-decision information L_i , which can be calculated as,

$$L_i = \log \frac{P_{B_i|Y}(0|y)}{P_{B_i|Y}(1|y)} = \log \frac{\sum_{x \in X_i^0} P_{Y|X}(y|x) P_X(x)}{\sum_{x \in X_i^1} P_{Y|X}(y|x) P_X(x)} \quad (1)$$

where $P_{B_i|Y}$ represents the probability that the bit is 0 or 1 for the known received symbol Y . X_i^0 and X_i^1 represent the symbol sets in which the i -th bit of the symbol is 0 or 1, $P_{Y|X}(y|x)$ is the conditional probability, and $P_X(x)$ is the prior probability. After L_i is given to the LDPC decoder, the output bit sequence is sorted. Then, the estimated bit sequences $\mathbf{b}(\mathbf{A})'$ and \mathbf{L}' are sent to the ELA decoder to perform the inverse operation of the DM. The final estimated uniform bit sequences \mathbf{U}_1' and \mathbf{U}_2' are used for the BER calculation.

Fig. 2 illustrates the mapping rule of PAM-8, where the blue and red numbers denote the amplitude bits and the sign bits, respectively. Next, the lookup table in the Table I with 2-symbol coding is used to yield a PS-PAM-8 signal. To implement the ELA-based DM in the Table I, a transmitted sequence is first divided into many 2-symbol segments. To avoid amounts of calculation and comparison on the original amplitude bits' energies, the ELA-based DM introduces the energy levels into the

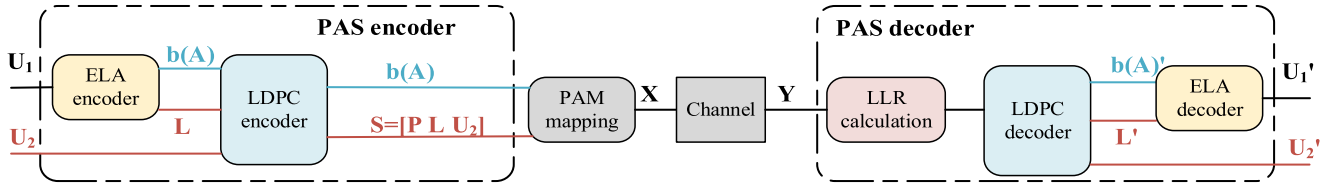


Fig. 1. Architecture of the PS-PAM-8 transmission system.

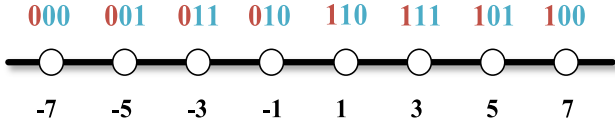


Fig. 2. The mapping rule of PAM-8 symbol.

TABLE I
LOOKUP TABLE OF ELA-BASED DM FOR PAM-8

U_1	E_1	$\mathbf{b(A)}$	E_2	\mathbf{L}
0000	98	1010	2	0
0001	74	1011	10	0
0010	50	1000	50	0
0011	58	1001	26	0
0100	74	1110	10	0
0101	50	1111	18	0
0110	26	0110	26	1
0111	34	0111	34	1
1000	50	0010	50	0
1001	26	1001	26	1
1010	2	1010	2	1
1011	10	1011	10	1
1100	58	0110	26	0
1101	34	1101	34	1
1110	10	1110	10	1
1111	18	1111	18	1

lookup table. Here, the energies of various 2-symbol segments are pre-calculated and classified into different energy levels and then energy-level mapping rule is assigned to yield variable probability distribution [26]. In the Table I, one combination contains amplitude bits of two PAM-8 symbols, i.e., 2-symbol coding. For example, ‘0001’ represents amplitude of “7” and “5”, with the amplitude bits of “00” and “01”. U_1 is the original uniform bits, and $\mathbf{b(A)}$ is PS encoded bits. E_1 and E_2 represent the energy of 2-symbol combination before and after ELA encoding, which is pre-calculated by summing the amplitude’ square of each symbol in the combination. \mathbf{L} is the label bits generated by ELA encoding, where “0” represents the inversion operation, as indicated by the blue numbers, and “1” represents no operation, as indicated by the black numbers. The inversion rules are shown in red numbers, i.e., “00” and “10”, and “01” and “11” are exchanged to each other. Here, the combination with higher energy levels is preferred to be inverted and the uniformity of label bits must be guaranteed.

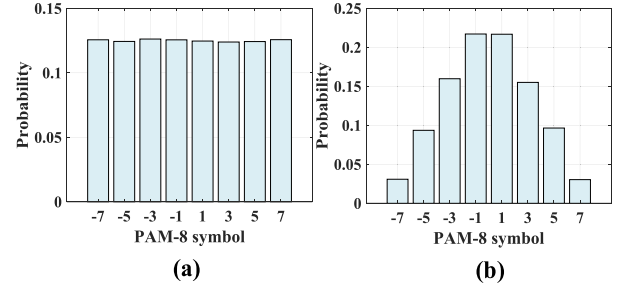


Fig. 3. Probability distribution histograms of (a) UN-PAM-8 (b) PS-PAM-8.

TABLE II
PARAMETERS OF UN-PAM-8 AND PS-PAM-8

<i>Parameter</i>	<i>UN-PAM-8</i>	<i>PS-PAM-8</i>
R_1	1	0.8
R_2	0.85	0.85
γ (w/o LDPC)	1	0.525
γ (w/ LDPC)	0.55	0.075
$H(A)$	2	1.736
R (w/o LDPC)	3	2.26
R (w/ LDPC)	2.55	1.811

Fig. 3 shows the probability distribution histograms of UN-PAM-8 signal and PS-PAM-8 signal. In comparison with of the uniform amplitude distribution of UN-PAM-8, PS-PAM-8 signal presents an approximate bilateral MB distribution. Since the PS signal improves the transmission performance at the expense of reduced information entropy, it is usually necessary to keep the net bit rate of the PS signal and the uniform signal the same for fair comparison. Generally, it can be achieved by increasing the baud rate of the PS signal. Table II lists the encoding parameters of UN-PAM-8 signal and PS-PAM-8. In the joint coding scheme, the code rate of each part is included and the LDPC will have a 15% redundancy. For the ELA-based DM, the code rate $R_1 = U_1/(U_1 + L)$, and the corresponding PS overhead is L/U_1 . In the 2-symbol ELA, the PS overhead is 20% and the overhead can be reduced by increasing the symbols of the ELA code segment. For the LPDC encoder, the code rate $R_2 = (U_1 + U_2 + L)/(U_1 + U_2 + L + P)$. The fraction of sign bits with information in the PS-PAM- M signal $\gamma = U_2/(U_2 + L + P)$. Besides, the fraction γ for UN-PAM- M signal is described as,

$$\gamma = 1 - (1 - R_2)m \quad (2)$$

where $m = \log_2(M)$.

The code rate R of joint coding is expressed as,

$$R = \frac{H(A^{n_c}) + H(S^{\gamma n_c})}{n_c} = H(A) + \gamma \quad (3)$$

where $H(A^{n_c})$ and $H(S^{\gamma n_c})$ represent the entropy of the amplitude bit and the sign bit with information for n_c symbols, respectively. In addition, $H(A)$ indicates the amplitude entropy after probability shaping [18]. Furthermore, the net bit rate is obtained by multiplying the code rate R and the baud rate of signal.

Although the PS-PAM-8 signal has stronger robustness than the UN-PAM-8 signal due to its non-uniform amplitude distribution, the equalizer is still indispensable to eliminate its channel impairments. The channel impairments of short-distance IM/DD signals are mainly caused by limited bandwidth of components, nonlinear distortion of system, fiber dispersion and system noise. Here, the bandwidth limitation usually results in the power fading at higher frequency, regarded as linear distortion. By contrast, the nonlinear distortion mainly comes from the non-ideal transfer characteristic of the modulator and the square-law detection of the photodetector (PD). The received PAM signal after PD detection can be written as,

$$y(t) = d_c^2 + |x(t) * h(t)|^2 + 2d_c x(t) * h(t) + n(t) \quad (4)$$

where $y(t)$ is the received signal, d_c is the direct current (DC) bias, $x(t)$ is the transmitted signal, $h(t)$ represents the channel response, and $n(t)$ is the system noise.

If the delay caused by the channel and the filter are not included, for the k -th symbol, the sampling value of $y(t)$ at time $t = kT_s$ can be given by,

$$y(kT_s) = d_c^2 + \left| x_k h(0) + \sum_{n \neq k} x_n h[(k-n)T_s] \right|^2 + 2d_c \left\{ x_k h(0) + \sum_{n \neq k} x_n h[(k-n)T_s] \right\} + n(t) \quad (5)$$

where $x_k h(0)$ is the sampling value of the k -th symbol, $\sum_{n \neq k} x_n h[(k-n)T_s]$ is the sum of the other symbols except the k -th symbol at the k -th sampling time. In (5), the first term is the DC component, the second term is the signal with nonlinear distortion, the third term is the signal with linear distortion, and the last term is the system noise. Therefore, the equalizer is applied to eliminate the nonlinear and linear ISI caused by the second and third terms. The Volterra series model is widely applied in nonlinear systems. By adjusting the tap coefficient, a VE can mitigate linear ISI as well as higher-order nonlinear ISI.

In this work, the FFE, the 2-order VE and the 2-order SVE are exploited to process the received signal, respectively. Here, the SVE is yielded by only keeping the kernel of 2-order VE to reduce the complexity of VE. Fig. 4 shows the structure of the 2-order VE, where the equalizer mainly is composed of the horizontally arranged delay unit T and the tap weighting coefficients. The FFE includes only the top half of the structure in Fig. 4. In order to eliminate both pre-ISI and post-ISI, the adjacent symbols will be included. The input signals of the above

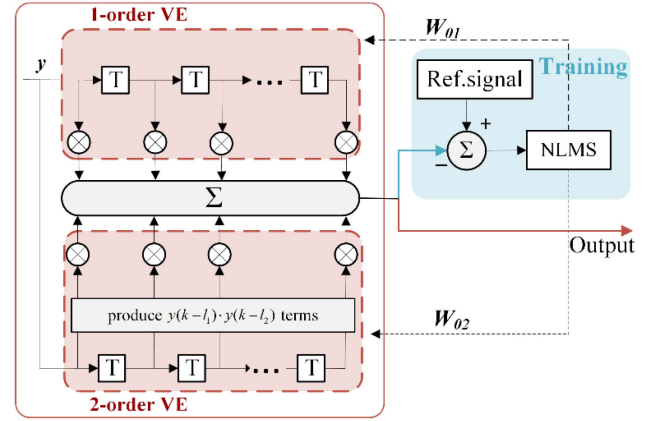


Fig. 4. Structure of 2-order Volterra equalizer.

equalizers are different, where Y_1 is the input of the FFE, Y_1 and Y_2 are the inputs of the 2-order VE and Y_1 and Y'_2 are the input of 2-order SVE, defined as,

$$\begin{aligned} Y_1 &= [y(k-N+1) \cdots y(k) \cdots y(k+N-1)] \\ Y_2 &= [y^2(k-M+1), y(k-M+1)y(k-M+2) \\ &\quad \cdots y(k-M+1)y(k+M-1) \\ &\quad \cdots \\ &\quad y^2(k), y(k)y(k+1) \cdots y(k)y(k+M-1) \\ &\quad \cdots \\ &\quad y^2(k+M-1)] \\ Y'_2 &= [y^2(k-M+1) \cdots y^2(k) \cdots y^2(k+M-1)] \end{aligned} \quad (6)$$

where $y(k)$ is the received k -th symbol, $2N-1$ is the memory length of FFE, and $2M-1$ is the nonlinear memory length of 2-order VE.

The equalized signals $d'(k)$ at the outputs of FFE, 2-order VE and 2-order SVE are written by

$$\begin{aligned} d'_{FFE}(k) &= \mathbf{W}_{01} Y_1 \\ &= \sum_{l_1=-N+1}^{N-1} w_{01}(l_1) y(k-l_1) \\ d'_{VE}(k) &= \mathbf{W}_{01} Y_1 + \mathbf{W}_{02} Y_2 \\ &= \sum_{l_1=-N+1}^{N-1} w_{01}(l_1) y(k-l_1) \\ &\quad + \sum_{l_1=-M+1}^{M-1} \sum_{l_2=-M+1}^{l_1} w_{02}(l_1, l_2) y(k-l_1) y(k-l_2) \end{aligned} \quad (7)$$

$$\begin{aligned} d'_{SVE}(k) &= \mathbf{W}_{01} Y_1 + \mathbf{W}_{02} Y'_2 \\ &= \sum_{l_1=-N+1}^{N-1} w_{01}(l_1) y(k-l_1) \end{aligned}$$

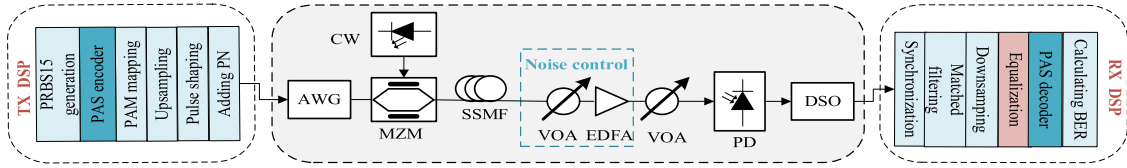


Fig. 5. Experimental setup of 20-Gbaud PS-PAM-8 transmission system.

$$+ \sum_{l_2=-M+1}^{M-1} w_{02}(l_2, l_2)y(k-l_2)y(k-l_2) \quad (9)$$

where W_{01} and W_{02} are vectors of tap coefficients. $y(k)$ is the received k -th symbol used as the input of the equalizer. l_i is the variable of memory length, w_{0i} is the tap coefficient of the i -th order VE. After the equalizer, the training symbols are extracted to calculate the difference between the desired output and the actual output. Then, the normalized least mean square (NLMS) algorithm with lower complexity is used to adjust the tap coefficients. The iterative training is implemented to obtain the optimum tap coefficients until the mean square error (MSE) approaches the convergence. Finally, the equalized output can be achieved by applying the obtained tap coefficients to the received testing symbols.

III. EXPERIMENTS AND RESULTS

Fig. 5 is the experimental setup of a PS-PAM-8 point-to-point transmission in the IDC network. At the transmitter, a pseudo-random binary sequence (PRBS) is first launched into the PAS encoder to generate the PS-PAM-8 signal after the bit-to-symbol mapping. The UN-PAM-8 signal can be directly mapped by skipping the PAS encoder. The PAS encoder includes an ELA encoder and an LDPC encoder. Then, the symbol sequence is upsampled to 2 samples per symbol (sps). Subsequently, a root raised cosine (RRC) finite impulse response (FIR) filter with a roll-off factor of 0.5 is used for pulse shaping. The roll-off factor will be reduced in higher baud-rate WDM PAM transmission system. Next, a pseudo-noise (PN) sequence is inserted for synchronization at the receiver. The data processed by the DSP at the transmitter is loaded into an arbitrary waveform generator (AWG), which has a 3-dB bandwidth of approximately 11 GHz. The baud rate of the transmitted signal can be adjusted by varying the sampling rate of the AWG and the maximum sampling rate of the AWG is 50 GSa/s. After that, the electrical PAM-8 signal from the AWG is modulated into a 1550.112 nm continuous wave (CW) laser by the Mach-Zehnder modulator (MZM). The modulated optical PAM-8 signal is launched into the fiber with the power of about 5.7 dBm. A variable optical attenuator (VOA) and an erbium-doped fiber amplifier (EDFA) are used to control the noise level for the BER measurement after transmission over 2-km of SSMF. The last VOA is used to regulate the optical power to the PD, where the PD has a 3-dB bandwidth of 10-GHz. The signal after optical-to-electrical conversion by the PD is acquired by a real-time oscilloscope (RTO) with a sampling rate of 50 GSa/s. The received data is first processed by the synchronization algorithm with correlation calculation.

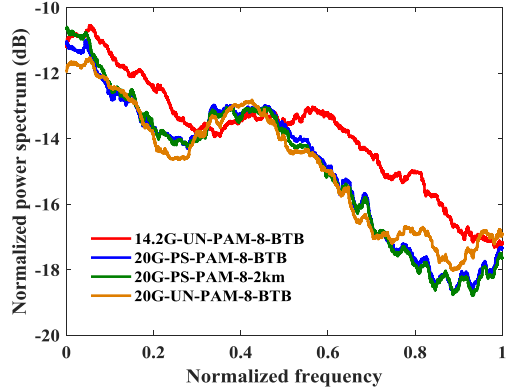


Fig. 6. Normalized power spectra of different PAM-8 signals at the receiver.

After that, the signal is re-sampled to 2 sps, and the matched filtering with the RRC FIR is utilized to yield the received signal with channel impairment. Next, the equalizer is introduced to restore the PAM-8 signal. Then, the PAS decoder is performed, including LLR calculation, LDPC decoder, and ELA decoder. The estimated bit sequence is obtained after LDPC decoder for post-FEC BER calculation, and for post-ELA BER calculation at the ELA decoder.

A. Performance Comparison of UN-PAM-8 and PS-PAM-8

First, the transmission performance of UN-PAM-8 signal and PS PAM-8 signal is investigated. In Fig. 6, the normalized power spectra of the 14.2-Gbaud UN-PAM-8, 20-Gbaud PS-PAM-8, 20-Gbaud UN-PAM-8 signals are plotted in the cases of back-to-back (BTB) and 2-km transmission to investigate the variation of the power spectra for different symbol rate and transmission length. It is obvious that the normalized spectra of the 20-Gbaud UN-PAM-8 signal and the 20-Gbaud PS-PAM-8 signal have similar trends. While at the same net bit rate, the spectrum of the 14.2-Gbaud UN-PAM-8 signal attenuates more slowly relative to that of the 20-Gbaud PS-PAM-8 signal. Therefore, the limited channel bandwidth has less influence on the 14.2-Gbaud UN-PAM-8 signal. Meanwhile, the chromatic dispersion induced by the 2-km SSMF transmission also has a negligible influence on the power spectra, as shown by blue and green curves in Fig. 6.

Fig. 7 shows the recovered symbols, eye diagram and power spectra of various signals with the conventional FFE. It is apparent that symbols with high amplitude levels are susceptible to the nonlinearity of the MZM. Although, the bandwidth limitation has a least impact to the 14.2-Gbaud UN-PAM-8 signal, which still suffers severer nonlinear impairment compared to the 20-Gbaud PS-PAM-8 signal. The recovered symbols of the

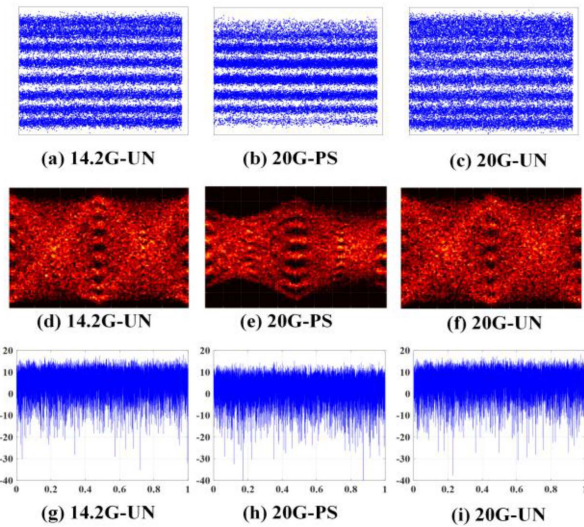


Fig. 7. Recovered symbols of different PAM-8 signals (ROP of -19 dBm): (a) 14.2-GBaud UN-PAM-8, (b) 20-GBaud PS-PAM-8, (c) 20-GBaud UN-PAM-8; eye diagram of different PAM-8 signals (ROP of -19 dBm): (d) 14.2-GBaud UN-PAM-8, (e) 20-GBaud PS-PAM-8, (f) 20-GBaud UN-PAM-8; and power spectra of different PAM-8 signals (ROP of -19 dBm): (g) 14.2-GBaud UN-PAM-8, (h) 20-GBaud PS-PAM-8, (i) 20-GBaud UN-PAM-8.

20-GBaud UN-PAM-8 signal is more dispersed relative to that of the 14.2-GBaud UN-PAM-8 signal due to the bandwidth limitation of components, as shown in Fig. 7(a) and (c). However, the PS-PAM-8 signal is mostly distributed at the symbols with the lower amplitude levels, and therefore the amplitude diagrams are relatively condensed, as shown in Fig. 7(b). In consequence, the eye opening of PS-PAM-8 is also much better compared to the other UN-PAM-8 signals, as shown in Fig. 7(d), (e) and (f). In addition, the FFE has compensated the power fading effect in all signals, and the power spectra are relatively flat as shown in Fig. 7(g), (h) and (i). It is worth noting that the power of the PS-PAM-8 signal is slightly lower than the other signals due to the overall energy reduction during PS encoding. Summarily, probabilistic shaping alleviates the impairments caused by the nonlinearity of the MZM by reducing the occurrence probability of symbols with high amplitude levels. Consequently, the 20-GBaud PS-PAM-8 signal outperforms the 14.2-GBaud UN-PAM-8 signal, although the bandwidth limitation has a larger influence on the PS signal due to the increased symbol rate.

Fig. 8 plots the measured BER curves as a function of received optical power (ROP) for 20-GBaud PS-PAM-8 and 14.2-GBaud UN-PAM-8 signals with the same net bit rate in the cases of BTB and 2-km SSMF transmissions after FFE. In the case of BTB, the post-FEC BER and post-ELA BER of the 20-GBaud PS-PAM-8 signal are shown by the dark-blue and light-blue square-marked solid curves in Fig. 8, where the ELA decoding is included in the post-ELA BER measurement. These two BER curves are very close to each other, which means that no error propagation occurs in the ELA. Therefore, the accurate transmission of the label bits has been achieved in the proposed joint encoding of ELA and LDPC scheme. The corresponding

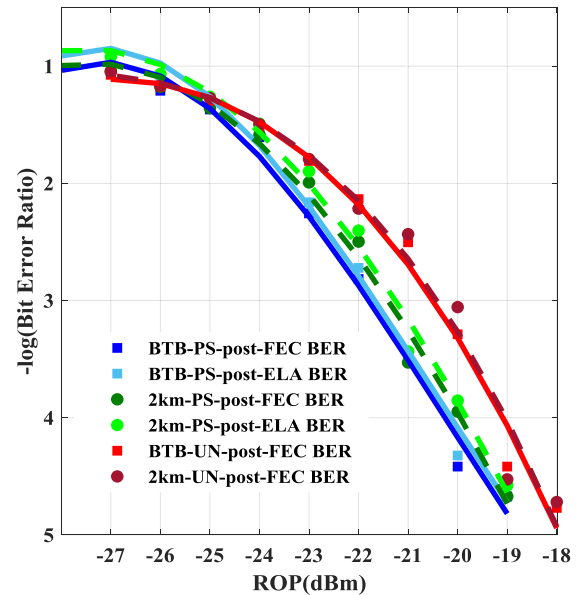


Fig. 8. Measured BER curves for 20-GBaud PS-PAM-8 and 14.2-GBaud UN-PAM-8 signal.

BER curves of the 20-GBaud PS-PAM-8 signal with 2-km SSMF transmission are shown by the dark-green and light-green circle-marked dashed curves in Fig. 8. It is obvious that the impairment caused by 2-km SSMF transmission is trivial due to the lower symbol rate. The UN-post-FEC BER curves show the measured BER performance of 14.2-GBaud UN-PAM-8 signal in the cases of BTB and 2-km SSMF transmission, as shown by the light-red square-marked solid curve and dark-red circle-marked dashed curves in Fig. 8. To sum up, at the same net bit rate, the high-baud-rate PS-PAM-8 signal has a better performance than that of the low-baud-rate UN-PAM-8 signal, where the signal isn't heavily bandwidth restricted and the ISI caused by the nonlinearity of the MZM is alleviated. However, when the symbol rate is increased significantly so that the signal is strictly bandwidth restricted, the situation will be different [10]. In addition, in conjunction with LDPC, the 20-GBaud PS-PAM-8 signal approaches the error-free convergence at the ROP of -18 dBm, while the 14.2-GBaud UN-PAM-8 requires -17 -dBm ROP to achieve the error-free performance.

B. Performance Comparison of FFE, VE and SVE

For PAM-8 signals, a simple equalizer is indispensable to yield the desired performance. For all equalizers, the memory length is a key parameter and longer memory length contributes to better performance at the expense of the computational complexity. In order to investigate the effect of memory length in various equalizers, we measured the post-FEC BER and post-ELA BER and calculated the number of multiplications to evaluate the performance and the complexity in Fig. 9 when the ROP is -21 dBm. Here, the post-FEC BER and post-ELA BER curves are shown in blue solid-circle-marked and hollow-circle-marked curves, respectively. The number of multiplications is plotted in red square-marked curves in Fig. 9. For the FFE in Fig. 9(a),

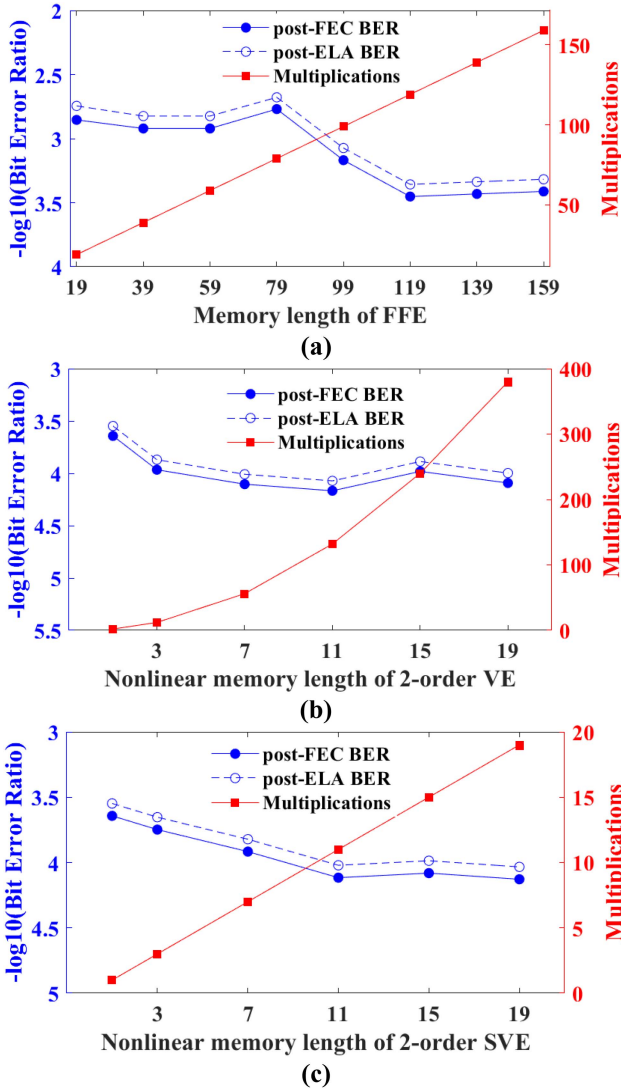


Fig. 9. The post-FEC BER, post-ELA BER and the number of multiplication curves versus memory length or non-linear memory length (-21 dBm): (a) FFE, (b) 2-order VE, (c) 2-order SVE.

the BER decreases as the memory length increases. Once the optimum BER performance is approached, there is no more benefit from the continuously increased memory length. However, the number of multiplications increases linearly with memory length. For the optimum BER performance, the memory length of FFE is chosen to be 119, as shown in Fig. 9(a). If the optimum BER is not required, the FFE only needs less than 19-taps. In the VE and SVE, besides the linear FFE, the nonlinear equalization is included. Thus, we investigate the effect of memory length for nonlinear equalization in the 2-order VE and 2-order SVE. The similar behaviors have been observed, as shown in Fig. 9(b) and (c). Fortunately, the number of multiplications increases linearly in the 2-order SVE instead of increasing quadratically as in the 2-order VE. Hence, the nonlinear memory length is set to 11 for both of 2-order VE and 2-order SVE to achieve the optimum BER performance.

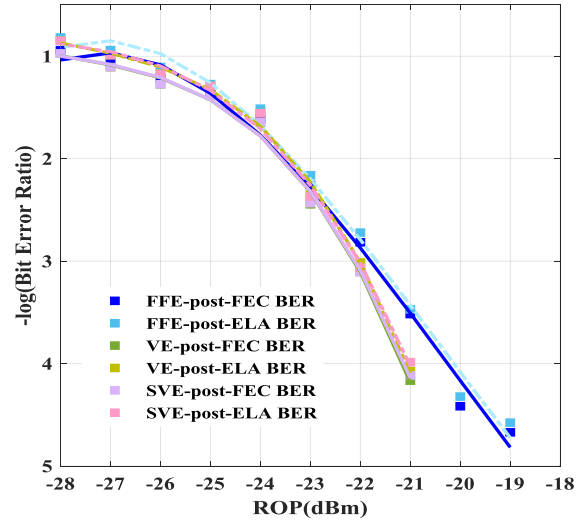


Fig. 10. Measured post-FEC BER and post-ELA BER curves with various equalizers for 20-GBaud PS-PAM-8 in the BTB transmission.

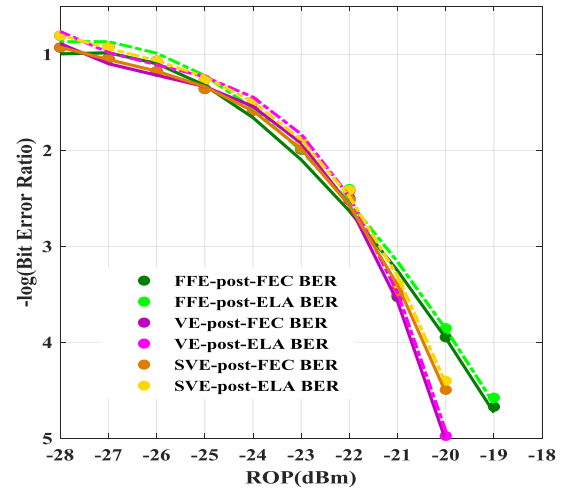


Fig. 11. Measured post-FEC BER and post-ELA BER curves with various equalizers for 20-GBaud PS-PAM-8 after 2-km SSMF transmission.

To compare the performance of various equalizers quantitatively, we measured post-FEC BER and post-ELA BER curves of 20-GBaud PS-PAM-8 signal with FFE, 2-order VE, and 2-order SVE in the BTB transmission, as shown in Fig. 10, where solid and dashed curves denote the post-FEC BER and the post-ELA BER. There is no error propagation in the proposed PS-PAM-8 system. The 2-order SVE with less complexity has achieved the similar BER performance as that of the 2-order VE and 2-dB receiver sensitivity improvement has been achieved for the error free performance in comparison with the FFE, as shown by green, pink and blue curves in Fig. 10.

To figure out the performance of various equalizers in the 2-km SSMF transmission system, the post-FEC BER and post-ELA BER curves of 20-GBaud PS-PAM-8 signal are measured in Fig. 11 and no error propagation is observed, as shown by solid and dashed curves. Similar as the BTB transmission, the 2-order VE and the 2-order SVE can achieve better BER performance

due to the additional nonlinear equalization, as shown by pink, yellow and green curves in Fig. 11. For the lower ROP, the system is dominated by the amplified spontaneous emission noise of EDFA during noise loading, all equalizers have the similar performance. With the increase of ROP, the 2-order VE and the 2-order SVE outperforms the FFE, as shown in Fig. 11. For longer SSMF transmission, higher-order VE and more components in (6) are indispensable to mitigate the PAM-8 signal degradation. Although, the signal degradation is small in the 2-km SSMF transmission, the 2-order VE with more components in (7) can achieve slightly better BER performance, as shown pink and yellow curves in Fig. 11. To sum up, the 2-order SVE and 2-order VE can approximately improve the receiver sensitivity of 2 dB compared to the FFE for the error free performance in the 20-GBaud PS-PAM-8 BTB transmission. By introducing the 2-km transmission, the improvement of receiver sensitivity is reduced to about 1dB because of uneliminated degradation from the fiber. Hence, the 2-order SVE is a promising equalizer for PS-PAM-8 signals in the short-reach intra-data-center networks.

C. Computational Complexity of FFE, VE and SVE

For the abovementioned equalizers, the complexity is evaluated based on the number of multiplications required by each symbol, which is highly depends on the memory length. Longer the memory length is and higher the complexity is. If the memory length of the FFE is designated as $2N - 1$, the pre- $(N - 1)$ symbols and the post- $(N - 1)$ symbols of the current symbol will be included. The computational complexity of C_{FFE} is given by,

$$C_{FFE} = 2N - 1 \quad (10)$$

Thus, the complexity linearly increases with the memory length.

For the VE with the 2-order memory length define as $2M - 1$, the computational complexity of C_{VE} is described as,

$$C_{VE} = 2N + 2M(2M - 1) - 1 \quad (11)$$

where the complexity is a quadratic function of the 2-order memory length $2M - 1$.

For the SVE, the kernel is only included and its complexity can be substantially reduced. The computational complexity of C_{SVE} is expressed as,

$$C_{SVE} = 2N + 2M - 2 \quad (12)$$

where the complexity rises linearly with the summation of the 1st-order and 2nd-order memory lengths.

IV. CONCLUSION

IM/DD PAM signals are good candidate for the intra-data-center optical interconnect. In comparison with conventional PAM-4 signals, PAM-8 signals have higher information entropy due to increased bits per symbol. However, PAM-8 signals are susceptible to various linear and nonlinear noise from transceivers and transmitted fibers. Fortunately, probabilistic shaping can improve the performance of PAM-8 systems by decreasing the occurrence probability of the symbols with high

amplitude levels. Meanwhile, the equalizer is also indispensable to mitigate the degradation induced by transceivers and transmitted fibers. Nevertheless, the conventional DMs and the equalizers used in the long-haul optical communication are quite complicated, which is not suitable for short-reach IM/DD PAM-8 signals. In order to escape the dilemma of performance and complexity, we propose and experimentally demonstrate a PS-PAM-8 transmission system with the joint coding of ELA-based DM and LDPC, and the simplified Volterra equalizer. ELA can realize an approximate bilateral MB distribution based on the simple lookup table by assigning energy level of various symbols. The post-FEC BER and post-ELA BER are measured to verify the feasibility of the proposed PS-PAM-8 system and the measured close post-FEC and post-ELA BER curves guarantees the performance of no error propagation in the proposed scheme. Furthermore, the simplified Volterra equalizer is exploited to improve the BER performance. Compared to the conventional FFE, the 2-order simplified Volterra equalizer has 2-dB and 1-dB improvements of receiver sensitivity in the BTB and 2-km SSMF transmission, respectively. Although the proposed PS-PAM-8 system is experimentally demonstrated in the 20-Gbaud system due to the shortage of large-bandwidth equipment, which can be used for the high-speed intra-data-center optical interconnect if the large-bandwidth components and equipment are available.

REFERENCES

- [1] K. Zhong et al., "Recent advances in short reach systems," in *Proc. IEEE Opt. Fiber Commun. Conf. Exhib.*, 2017, pp. 1–3.
- [2] K. Zhong, X. Zhou, J. Huo, C. Yu, C. Lu, and A. Lau, "Digital signal processing for short-reach optical communications: A review of current technologies and future trends," *J. Lightw. Technol.*, vol. 36, no. 2, pp. 377–400, Jan. 2018.
- [3] L. Zhang, J. Wei, N. Stojanovic, C. Prodaniuc, and C. Xie, "Beyond 200-Gb/s DMT transmission over 2-km SMF based on a low-cost architecture with single-wavelength, single-DAC/ADC and single-PD," in *Proc. IEEE Eur. Conf. Opt. Commun.*, 2018, pp. 1–3.
- [4] J. Wei et al., "Experimental comparison of modulation formats for 200 G/λ IMDD data center networks," in *Proc. IEEE 45th Eur. Conf. Opt. Commun.*, 2019, pp. 1–4.
- [5] M. Xiang et al., "Advanced DSP enabled C-band 112 Gbit/s/λ PAM-4 transmissions with severe bandwidth-constraint," *J. Lightw. Technol.*, vol. 40, no. 4, pp. 987–996, Feb. 2022.
- [6] J. Zhang et al., "C-band 120-Gb/s PAM-4 transmission over 50-km SSMF with improved weighted decision-feedback equalizer," *Opt. Exp.*, vol. 29, no. 25, pp. 41622–41633, Dec. 2021.
- [7] M. Yin, D. Zou, W. Wang, F. Li, and Z. Li, "Transmission of a 56 Gbit/s PAM4 signal with low-resolution DAC and pre-equalization only over 80 km fiber in C-band IM/DD systems for optical interconnects," *Opt. Lett.*, vol. 46, no. 22, pp. 5615–5618, Nov. 2021.
- [8] N. Stojanovic, F. Karinou, Z. Qiang, and C. Prodaniuc, "Volterra and Wiener equalizers for short-reach 100G PAM-4 applications," *J. Lightw. Technol.*, vol. 35, no. 21, pp. 4583–4594, Nov. 2017.
- [9] T. Eriksson, M. Chagnon, F. Buchali, K. Schuh, S. Brink, and L. Schmalen, "56 Gbaud probabilistically shaped PAM8 for data center interconnects," in *Proc. IEEE Eur. Conf. Opt. Commun.*, 2017, pp. 1–3.
- [10] M. Hossain et al., "Experimental comparison of uniform and probabilistically shaped PAM-8 for IMDD system at transmission rates beyond 200 Gbit/s," in *Proc. IEEE Opt. Fiber Commun. Conf. Exhib.*, 2021, pp. 1–3.
- [11] M. S. Bin Hossain et al., "Experimental comparison of cap and cup probabilistically shaped PAM for O-Band IM/DD transmission system," in *Proc. IEEE Eur. Conf. Opt. Commun.*, 2021, pp. 1–4.
- [12] J. Zhang et al., "Demonstration of 260-Gb/s single-lane EML-based PS-PAM-8 IM/DD for datacenter interconnects," in *Proc. IEEE Opt. Fiber Commun. Conf. Exhib.*, 2019, pp. 1–3.

- [13] H. Taniguchi et al., “225-Gbps/λ PAM-8 transmission over 2-km using 4-λ LAN-WDM TOSA with MLSE based on nonlinear channel estimation,” in *Proc. IEEE Opto-electron. Commun. Conf.*, 2020, pp. 1–3.
- [14] T. Wettlin et al., “Low-complexity nonlinearity compensation for short-reach IM/DD systems using PAM,” in *Proc. IEEE Opt. Fiber Commun. Conf. Exhib.*, 2021, pp. 1–3.
- [15] X. Chen et al., “Single-wavelength and single-photodiode 700 Gb/s entropy-loaded PS-256-QAM and 200-GBaud PS-PAM-16 transmission over 10-km SSMF,” in *Proc. IEEE Eur. Conf. Opt. Commun.*, 2020, pp. 1–4.
- [16] J. Zhang et al., “Demonstration of single-lane 350-Gb/s PS-PAM-16 in the C-band using single-DAC for data center interconnects,” in *Proc. IEEE Opt. Fiber Commun. Conf. Exhib.*, 2021, pp. 1–3.
- [17] X. Wu, J. Zhang, Q. Yan, A. P. T. Lau, and C. Lu, “C-band single-lane 290.4-Gb/s net rate PS-PAM-16 transmission over 1-km SSMF using low-complexity nonlinear equalization and single DAC,” in *Proc. Conf. Lasers Electro-Opt.*, 2022, pp. 1–2.
- [18] G. Böcherer, F. Steiner, and P. Schulte, “Bandwidth efficient and rate-matched low-density parity-check coded modulation,” *IEEE Trans. Commun.*, vol. 63, no. 12, pp. 4651–4665, Dec. 2015.
- [19] G. Böcherer, P. Schulte, and F. Steiner, “Probabilistic shaping and forward error correction for fiber-optic communication systems,” *J. Lightw. Technol.*, vol. 37, no. 2, pp. 230–244, Jan. 2019.
- [20] G. Böcherer, P. Schulte, and F. Steiner, “Probabilistic shaping benefits and practicality for higher-order QAM,” in *Proc. IEEE Photon. Con. (IPC)*, 2017, p. 93.
- [21] T. Yoshida, M. Karlsson, and E. Agrell, “Hierarchical distribution matching for probabilistically shaped coded modulation,” *J. Lightw. Technol.*, vol. 37, no. 6, pp. 1579–1589, Mar. 2019.
- [22] P. Schulte and G. Böcherer, “Constant composition distribution matching,” *IEEE Trans. Inf. Theory*, vol. 62, no. 1, pp. 430–434, Jan. 2016.
- [23] T. Ramabadran, “A coding scheme for m-out-of-n codes,” *IEEE Trans. Commun.*, vol. 38, no. 8, pp. 1156–1163, Aug. 1990.
- [24] J. Cho, “Prefix-free code distribution matching for probabilistic constellation shaping,” *IEEE Trans. Commun.*, vol. 68, no. 2, pp. 670–682, Feb. 2020.
- [25] J. Cho, S. Chandrasekhar, R. Dar, and P. Winzer, “Low-complexity shaping for enhanced nonlinearity tolerance,” in *Proc. IEEE Eur. Conf. Opt. Commun.*, 2016, pp. 1–3.
- [26] M. Liu, M. Gao, and J. Ke, “Multi-distributed probabilistically shaped PAM-4 system for intra-data-center networks,” *Chin. Opt. Lett.*, vol. 19, no. 11, Nov. 2021, Art. no. 110604.
- [27] T. Wettlin, S. Calabrò, T. Rahman, J. Wei, N. Stojanovic, and S. Pachnicke, “DSP for high-speed short-reach IM/DD systems using PAM,” *J. Lightw. Technol.*, vol. 38, no. 24, pp. 6771–6778, Dec. 2020.
- [28] D. Zou et al., “100G PAM-6 and PAM-8 signal transmission enabled by pre-chirping for 10-km Intra-DCI utilizing MZM in C-band,” *J. Lightw. Technol.*, vol. 38, no. 13, pp. 3445–3453, Jul. 2020.
- [29] M. Hossain et al., “Feasibility of transmitting 270 Gbit/s with PAM-8 in O-band CWDM4 with IM/DD system,” in *Proc. IEEE Opt. Fiber Commun. Conf. Exhib.*, 2021, pp. 1–3.
- [30] Y. Zhu, L. Li, X. Miao, Q. Wu, L. Yin, and W. Hu, “100G PAM-8 transmission with direct detection utilizing imbalanced Mach-Zehnder modulator for power fading suppression,” in *Proc. IEEE 19th Int. Conf. Commun. Netw.*, 2021, pp. 1–3.
- [31] X. Tang, Y. Qiao, Y. Chen, Y. Lu, and G. Chang, “Digital pre- and post-equalization for C-band 112-Gb/s PAM4 short-reach transport systems,” *J. Lightw. Technol.*, vol. 38, no. 17, pp. 4683–4690, Sep. 2020.
- [32] R. Fischer, *Precoding and Signal Shaping for Digital Transmission*. Hoboken, NJ, USA: Wiley, 2002.
- [33] D. Li et al., “Low-complexity equalization scheme for suppressing FFE-enhanced in-band noise and ISI in 100 Gbps PAM4 optical IMDD system,” *Opt. Lett.*, vol. 45, no. 9, pp. 2555–2558, May 2020.
- [34] N. Eiselt et al., “Experimental demonstration of 112-Gbit/s PAM-4 over up to 80 km SSMF at 1550 nm for inter-DCI applications,” in *Proc. IEEE 42nd Eur. Conf. Opt. Commun.*, 2016, pp. 1–3.
- [35] H. Y. Rha, S.-R. Moon, H.-S. Kang, S.-W. Lee, I.-K. Hwang, and J. K. Lee, “Low-complexity soft-decision Viterbi algorithm for IM/DD 56-Gb/s PAM-4 system,” *IEEE Photon. Technol. Lett.*, vol. 31, no. 5, pp. 361–364, Mar. 2019.
- [36] R. Rath, D. Clausen, S. Ohlendorf, S. Pachnicke, and W. Rosenkranz, “Tomlinson–Harashima precoding for dispersion uncompensated PAM-4 transmission with direct-detection,” *J. Lightw. Technol.*, vol. 35, no. 18, pp. 3909–3917, Sep. 2017.
- [37] Q. Hu, R. Dischler, K. Schuh, H. Buelow, L. Schmalen, and F. Buchali, “Beating bandwidth limitation for high-speed PAM-4 transmission based on turbo equalizer,” in *Proc. IEEE Eur. Conf. Opt. Commun.*, 2017, pp. 1–3.
- [38] M. S.-B. Hossain et al., “Transmission beyond 200 Gbit/s with IM/DD system for campus and intra-datacenter network applications,” *IEEE Photon. Technol. Lett.*, vol. 33, no. 5, pp. 263–266, Mar. 2021.